



UNICA

UNIVERSITÀ  
DEGLI STUDI  
DI CAGLIARI



Università di Cagliari

UNICA IRIS Institutional Research Information System

**This is the Author's manuscript version of the following contribution:**

M. Lai, S.R. Eugster, E. Reccia, M. Spagnuolo, A. Cazzani, "Corrugated shells: An algorithm for generating double-curvature geometric surfaces for structural analysis", *Thin-Walled Structures*, **173**(1), 2022, art. # 109019, pp 1-11

**The publisher's version is available at:**

<https://dx.doi.org/10.1016/j.tws.2022.109019>

**When citing, please refer to the published version.**

This full text was downloaded from UNICA IRIS <https://iris.unica.it/>

1  
2  
3  
4  
5  
6  
7  
8  
9  
10  
11  
12  
13  
14

# Corrugated shells: an algorithm for generating double-curvature geometric surfaces for structural analysis

15  
16  
17

M. Lai<sup>a,b,\*</sup>, S. R. Eugster<sup>b</sup>, E. Reccia<sup>a</sup>, M. Spagnuolo<sup>a</sup>, A. Cazzani<sup>a</sup>

18  
19

<sup>a</sup>*Dipartimento di Ingegneria Civile Ambientale e Architettura, Università degli Studi di  
Cagliari, Cagliari, Italy*

20  
21

<sup>b</sup>*Institute for Non-Linear Mechanics, University of Stuttgart, Stuttgart, Germany*

---

22  
23  
24

## Abstract

25  
26  
27  
28  
29  
30  
31  
32  
33  
34  
35  
36  
37  
38  
39  
40  
41  
42  
43

Analysis of corrugated shell structures is an interesting problem in Structural Mechanics, which has many practical applications in Civil Engineering and Architecture. Thanks to corrugation, these structures have a remarkable feature: the wavy (undulated) shape in their edge provides significant enhancements in their structural behaviour, increasing the bending stiffness at the edge and allowing for a non-negligible reduction of its thickness. Moreover, looking at the non-linear behaviour, domes corrugation plays a relevant role in instability phenomena, such as the influence of imperfections and increasing resistance to snap-through.

44  
45  
46  
47  
48  
49  
50  
51  
52

A problem in the study of such kind of shells is the definition of mathematical and geometrical model and the construction of a suitable mesh to perform FE analyses. The aim of this paper is to find an automated way to generate a double-curvature geometric surface that can be used both in

---

53  
54

\*Corresponding author

55  
56  
57

*Email address:* [matteolai@unica.it](mailto:matteolai@unica.it) (M. Lai)

1  
2  
3  
4  
5  
6  
7  
8  
9 static and in non-linear stability analyses of such corrugated shell structures.  
10 A method to generate a NURBS surface, suitable for a parametric FE analy-  
11 sis from a geometrical model expressed in a parametric form, is proposed and  
12 applied to a shell inspired by the well-known dome designed by Pier Luigi  
13 Nervi in 1959 for the roof of the Palasport Flaminio in Rome.  
14  
15  
16  
17

18 *Keywords:* corrugated shells, shallow shells, domes, Palasport Flaminio,  
19 Pier Luigi Nervi  
20  
21  
22

---

## 23 24 **1. Introduction**

25  
26 The problem presented in this work concerns the structural analysis of  
27 corrugated shell structures. These structures have a remarkable character-  
28 istic: the wavy shape of their edge gives a significant improvement to their  
29 structural behaviour, increasing the bending stiffness at the edge, thus allow-  
30 ing the designer to reduce its thickness. A problem in studying this structural  
31 typology is how to deal with its complex geometry. This paper aims to find  
32 an automated way to generate a double-curvature geometric surface, given  
33 its mathematical description, which can be used both in static and non-linear  
34 stability analyses of corrugated shell structures.  
35  
36  
37  
38  
39  
40  
41  
42  
43

44 For properly treating this topic, it is useful to recall a state-of-the-art  
45 where the problem studied in the present work can be framed. Some rele-  
46 vant examples in the field of corrugated shell structures can be found along  
47 the history of Civil Engineering. In East Anglia (England) from XVII un-  
48 til XIX century wavy fences were largely built as garden walls, known as  
49 *Crinckle crankle walls* (see Fig. 1). Some of them still exist in Suffolk and  
50 Hampshire. This kind of construction, which has been attributed to Dutch  
51  
52  
53  
54  
55  
56  
57  
58  
59  
60  
61  
62  
63  
64  
65

1  
2  
3  
4  
5  
6  
7  
8  
9  
10  
11  
12  
13  
14  
15  
16  
17  
18 engineers [1], presents a wavy shape that provides the wall with bending  
19 stiffness and improves its structural response to horizontal loads. As a con-  
20 sequence, bricklayers could build a slender wall made of a single line of bricks  
21 without the need for abutments or buttresses. The effect of corrugation, then,  
22 is to improve the mechanical behaviour of this structure. The same remark  
23 will also be true for shells, as it will be clear in the following. Specifically,  
24 one can observe corrugation in seashell structures arising as a result of opti-  
25 mization processes.

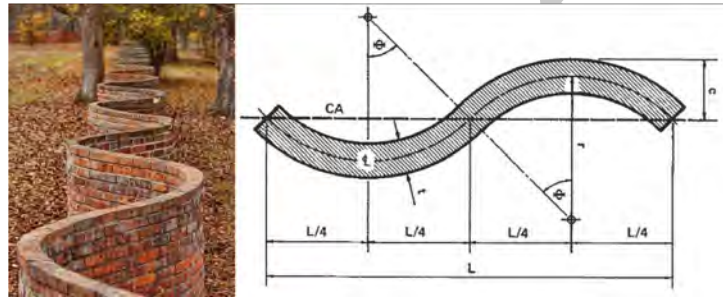


Figure 1: A Crinkle Crinkle wall in Suffolk (UK), left. A sketch of the same wall, right.

26  
27  
28  
29  
30  
31  
32  
33  
34  
35  
36  
37  
38  
39  
40  
41  
42  
43  
44  
45  
46  
47  
48  
49  
50  
51  
52  
53  
54  
55  
56  
57  
58  
59  
60  
61  
62  
63  
64  
65

Indeed, corrugated shells can be found in nature: structures of such type can be obtained by a topologic optimization process, as those occurring in bone reconstruction (see, for example, [2–4]). A relevant example, also of interest for the topic of the present work, is represented by seashells. It is observed that the mussel minimizes the effort in building its dwelling changing from a smooth to a corrugated shape [5]. The outcome of the new smart shape is to increase the mechanical resistance with the same amount of material. As a consequence, the optimized structure is said to be shape-resistant. The study presented herein is motivated by similar considerations related to efficiency

1  
2  
3  
4  
5  
6  
7  
8  
9  
35 and resistance criteria.

10  
11 On the Civil Engineering side, the need for corrugated shells or plates  
12  
13 is also motivated by structural efficiency. The main differences between  
14  
15 the Civil Engineering case and other fields (such as the cited example of  
16  
17 seashells) consist in scale and, clearly, in the employed materials. Generally  
18  
19 in Civil Engineering and Architecture a standard material is reinforced con-  
20  
21 crete (shortly, RC), whose high-performance dissipation properties are also  
22  
23 known, as it was pointed out in [6–8]. In addition, special attention should  
24  
25 be given to the durability of this material, [9–11].

26  
27 RC has always been an excellent material to be used in optimized [11],  
28  
29 [12] and customized-shaped building [13], also in the Italian school of Struc-  
30  
31 tural Engineers, which between the '50s and '70s was led by Pier Luigi Nervi  
32  
33 and Sergio Musmeci. An outstanding piece of Italian architecture, where a  
34  
35 corrugated shell made of reinforced concrete is used, is the roof of a gasoline  
36  
37 station in Sesto San Giovanni (Milano), designed by Aldo Favini in 1949,  
38  
39 which was unfortunately destroyed some years later. Then this type of con-  
40  
41 struction has been progressively fallen into disuse, due to the increase in the  
42  
43 cost of the formwork and scaffolding.

44  
45 As it has been already remarked, some models can be suitably adapted to  
46  
47 apparently different structures. Referring to Fig. 2, one can observe different  
48  
49 objects where corrugation has a relevant role: potentially the spirit of the  
50  
51 present work is to develop an algorithm which is useful for all these cases,  
52  
53 independently on the scale or material. An extensive body of literature exists  
54  
55 and deals with the connection between form and structure, and these topics  
56  
57 are covered in foremost books like [14, 15]. A new gaze is provided from  
58  
59

1  
2  
3  
4  
5  
6  
7  
8  
9  
60 the SIXXI project, whose purpose is to give a distinct point of view on the  
10  
61 Italian school of Structural Engineering, and is set out in [16]. Even though  
11  
12 primary source can be found in Nervi's book [17], some recent advancements  
13  
62  
14  
63 have been provided in [18, 19]. The inspiration for this work has been taken  
15  
16  
64 from one of Nervi's works: the shallow shell designed for Rome Olympics  
17  
18  
65 game in 1960 to cover the roof of the Palazzetto dello Sport or, shortly,  
19  
20  
66 *Palasport Flaminio* (from the name of the district of Rome where it was  
21  
22  
67 built and still stands nowadays).



23  
24  
25  
26  
27  
28  
29  
30  
31  
32  
33  
34  
35  
36  
37  
38  
39  
40  
41  
42  
43 Figure 2: Example of corrugated shells: (a) Nervi's Palasport Flaminio dome, (b) Hobermann  
44  
45 deployable structure, (c) Favini's roof, (d) corrugated sea-shells.

46  
47  
48  
68 Nervi's shell is a foremost piece of unique architecture and it also constitutes  
49  
50  
69 an inexhaustible source for structural design, even in different fields. For  
51  
52  
70 instance, it has been a source of influence for the Iris Dome retractable roof,  
53  
54  
71 which was designed by Charles Hobermann [20]. This kind of corrugated  
55  
56  
72 shapes, known as *umbrella-type surfaces*, can be studied from a mathematical

1  
2  
3  
4  
5  
6  
7  
8  
9  
73 point of view as it has been done, in a more general framework, in [21].

10  
11 One can employ a representation of 2-D surfaces in Cartesian coordinates  
12  
13 depending on a set of parameters defined in a closed interval. A comprehen-  
14  
15 sive guide for a wide variety of parametric equations can be found in [22].  
16

17 From a Structural Mechanics point of view, the consequences of corruga-  
18  
19 tions in building structures have not yet been entirely investigated, perhaps  
20  
21 due to the intrinsic difficulties to manage the mathematical implications of  
22  
23 corrugation. Some theoretical background is given for static analyses in [23]  
24  
25 and considerations about the stability and multi-stability of open corrugated  
26  
27 shell are pointed out in [24]. In [25] it is possible to find a parametric analy-  
28  
29 sis devoted to understanding the role of corrugation in improving the seismic  
30  
31 resistance of vaults and domes.

32 In [26–29] some relevant results in the field of shells were set out. These  
33  
34 studies can be useful also for generalizing the results presented in this work [30–  
35  
36 34].  
37

38 Frequently, in Architecture it is needed to design large-span roofs: to this  
39  
40 aim, the theory of shells provides the most effective approach, introducing  
41  
42 structural problems that need to be properly taken into account. A remark-  
43  
44 able problem consists in enhancing the structural resistance. This can be  
45  
46 made in different ways, as, for instance, by increasing the thickness of the  
47  
48 shell surface or by placing a ring-beam on the shell edge. In this context  
49  
50 a smarter solution (also from an architectural and aesthetics point of view)  
51  
52 consists in employing corrugated shell surfaces which allow in reducing the  
53  
54 shell thickness.

55 The above recalled literature is necessary to address the main aim of this  
56  
57  
58  
59  
60  
61  
62  
63  
64  
65

1  
2  
3  
4  
5  
6  
7  
8  
9  
10 98 paper: to recognise the influence of corrugations in the mechanics of shells,  
11 99 taking into account relevant non-linear effects affecting slender and shal-  
12  
13 100 low shells, whose edge is wavy-corrugated. Non-linear behaviour remarkably  
14  
15 101 affects the shell mechanical performances, such as snap-through mechanism  
16  
17 102 and buckling instability phenomena [35–42]. A successfully employed method  
18  
19 103 in dealing with this kind of problem consists in using a set of safety factors  
20  
21 104 to knock down the theoretical results: see for example the NASA aeronautics  
22  
23 105 recommendations [43].

24  
25 106 The first step for performing a correct numerical analysis is to set a pro-  
26  
27 107 cedure which can produce geometrical objects replicating the mathematical  
28  
29 108 dome shape in a process suitable for structural analysis using doubly-curved  
30  
31 109 elements. In Section 2 the geometrical representation of a corrugated shell is  
32  
33 110 introduced in such a way that mathematical parametric equations are given.  
34  
35 111 In Section 3 an algorithm to represent a NURBS based surface is presented.  
36  
37 112 Numerical results are shown and discussed in Section 4 in order to investi-  
38  
39 113 gate the influence of shell corrugation. Finally, in Section 5, some concluding  
40  
41 114 remarks are presented.

## 42 43 115 **2. Wavy-edge shell parametric description**

44  
45  
46 116 In this section, a mathematical description of a wavy-edge surface inspired  
47  
48 117 to the Nervi's Palasport Flaminio dome is proposed. Its equations depend on  
49  
50 118 several parameters which control the corrugation shape along the shell side.

51  
52 119 The adopted spherical polar reference system is shown in Fig. 3, where  $r$   
53  
54 120 is the radial distance from the pole,  $\vartheta$  is the colatitude angle (the complement  
55  
56 121 to the latitude angle) and  $\varphi$  is the longitude angle. So, a generic point  $P$ ,



1  
2  
3  
4  
5  
6  
7  
8  
9  
10  
11  
12  
13  
14  
15  
16  
17  
18  
19  
20  
21  
22  
23  
24  
25  
26  
27  
28  
29  
30  
31  
32  
33  
34  
35  
36  
37  
38  
39  
40  
41  
42  
43  
44  
45  
46  
47  
48  
49  
50  
51  
52  
53  
54  
55  
56  
57  
58  
59  
60  
61  
62  
63  
64  
65

122 belonging to the 3-D space, is uniquely identified by its spherical coordinates  
123  $(r, \vartheta, \varphi)$ . A parametric representation of a wavy-edge spherical shell can be  
124 given introducing a parametrization of its radius. A surface could thus be  
125 described by using two parameters only, viz.  $\vartheta$  and  $\varphi$ , where each pair  $(\vartheta_i,$   
126  $\varphi_i)$  describes a point  $P_i$  which belongs to the surface.

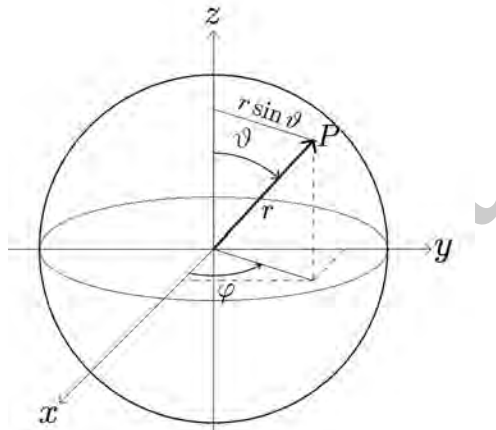


Figure 3: Spherical polar coordinate system.

127 Considering a perfect spherical shell, whose radius is  $R_0$ , its *parametric equa-*  
128 *tions* are the classical ones

$$\left\{ \begin{array}{l} x = R_0 \sin \vartheta \cos \varphi \\ y = R_0 \sin \vartheta \sin \varphi \\ z = R_0 \cos \vartheta. \end{array} \right. \quad (1)$$

130 From Eq. (1), by squaring and summing up (term by term) both sides, pa-  
131 rameters  $\vartheta$  and  $\varphi$  can be eliminated and the resulting *implicit* representation

1  
2  
3  
4  
5  
6  
7  
8  
9  
10  
11  
12  
13  
14  
15  
16  
17  
18  
19  
20  
21  
22  
23  
24  
25  
26  
27  
28  
29  
30  
31  
32  
33  
34  
35  
36  
37  
38  
39  
40  
41  
42  
43  
44  
45  
46  
47  
48  
49  
50  
51  
52  
53  
54  
55  
56  
57  
58  
59  
60  
61  
62  
63  
64  
65

132 of the spherical surface is obtained:

$$133 \quad x^2 + y^2 + z^2 - R_0^2 = 0. \quad (2)$$

134 Now, recalling that the radial distance  $r$  from the pole is given, in terms of  
135 Cartesian coordinates by:

$$r = \sqrt{x^2 + y^2 + z^2},$$

136 an *explicit* representation of the spherical surface results:

$$137 \quad r = R_0. \quad (3)$$

138 Looking at Eq. (3) it is apparent that in the case of a sphere the radial  
139 distance of any point of the surface is independent of the spherical coordinates  
140  $\vartheta, \varphi$ . This consideration suggests an easy way to construct a surface, shaped  
141 as a portion of a hemispherical shell but exhibiting a corrugation on the  
142 edge. Indeed such corrugated edge can be treated as a perturbation of the  
143 constant radius  $R_0$ , resulting in a wavy-edge. Then, for such surface the  
144 radius  $r = r(\vartheta, \varphi)$  may be represented as

$$145 \quad r = R_0 [1 + f(\vartheta)g(\varphi)]. \quad (4)$$

146 In Eq. (4) the perturbation is made up by two factors: the former  $f(\vartheta)$ ,  
147 depends only on colatitude  $\vartheta$  and gives the shape of the perturbed meridian,  
148 while the latter  $g(\varphi)$  depends only on the longitude angle  $\varphi$  and modulates the  
149 form of all parallels. In order to get a cyclic symmetry along each parallel line,  
150 function  $g(\varphi)$  must be periodic; a suitable choice to get a smooth repetition  
151 by a whole number  $n$  of a basic wave pattern is then:

$$152 \quad g(\varphi) = \cos(n\varphi). \quad (5)$$

1  
2  
3  
4  
5  
6  
7  
8  
9  
10  
11  
12  
13  
14  
15  
16  
17  
18  
19  
20  
21  
22  
23  
24  
25  
26  
27  
28  
29  
30  
31  
32  
33  
34  
35  
36  
37  
38  
39  
40  
41  
42  
43  
44  
45  
46  
47  
48  
49  
50  
51  
52  
53  
54  
55  
56  
57  
58  
59  
60  
61  
62  
63  
64  
65

153 This ensures that an undulated wave is repeated  $n$  times along the surface  
154 edge, i.e. the period of function  $g$  is simply  $2\pi/n$ ; in order to obtain that  
155 the fundamental (or *zero*) meridian  $\varphi = 0$  is indeed perturbed with reference  
156 to the spherical shape, the cosine function has been preferred to its sine  
157 counterpart.

158 Function  $f(\vartheta)$ , which controls the perturbation of the radius along the merid-  
159 ian with reference to that of a perfect sphere,  $R_0$ , can be chosen in several  
160 ways. A possible choice is:

$$161 \quad f(\vartheta) = aH(\vartheta - \vartheta_0) \left( \frac{\vartheta - \vartheta_0}{\vartheta_0} \right)^2. \quad (6)$$

162 In Eq. (6)  $a$  is a parameter controlling the amplitude of the perturbation,  $H$   
163 is Heaviside step function (or unit step function), defined as:

$$H(\vartheta - \vartheta_0) = \begin{cases} 1, & \text{if } \vartheta \geq \vartheta_0 \\ 0, & \text{if } \vartheta < \vartheta_0, \end{cases}$$

164 whose role is to switch on the radius perturbation in correspondence of  $\vartheta_0$ ,  
165 namely the colatitude angle at which such perturbation originates. Finally  
166 the term  $(\vartheta - \vartheta_0)^2/\vartheta_0^2$  has been introduced to produce a smooth variation  
167 of  $r$  along the meridian in a neighborhood of  $\vartheta_0$ . Despite the presence of  
168 Heaviside's step function, it comes out from Eq. (6) that the resulting radius  
169  $r(\vartheta, \varphi)$  is an almost everywhere continuous and differentiable function of its  
170 arguments.

171 If a smoother shape is desired, the unit step function  $H$  can be replaced  
172 by a continuously differentiable function approximating it, like, for instance,

1  
2  
3  
4  
5  
6  
7  
8  
9 the hyperbolic tangent; consequently, in this case,  $f(\vartheta)$  can be expressed by:

10  
11  
12  
13  
14  
15  
16  
17  
18  
19  
20  
21  
22  
23  
24  
25  
26  
27  
28  
29  
30  
31  
32  
33  
34  
35  
36  
37  
38  
39  
40  
41  
42  
43  
44  
45  
46  
47  
48  
49  
50  
51  
52  
53  
54  
55  
56  
57  
58  
59  
60  
61  
62  
63  
64  
65

$$f(\vartheta) = \frac{a}{2} [1 + \tanh(b(\vartheta - \vartheta_0))], \quad (7)$$

175 where  $a$  is again a parameter controlling the amplitude of the perturbation,  
176 while  $b$  is a second parameter which, when increases, makes steeper the graph  
177 of the function and allows approximating, with the desired accuracy, a step  
178 function with a continuous one.

179 A mathematical representation of the corrugated surface is then given  
180 by updating the previously mentioned equations of a hemispherical shell,  
181 using  $r(\vartheta, \varphi)$  defined by Eq. (4) instead of the constant radius  $R_0$ . As a  
182 consequence, the parametric equations of the corrugated surface become:

$$\begin{cases} x = r(\vartheta, \varphi) \sin \vartheta \cos \varphi \\ y = r(\vartheta, \varphi) \sin \vartheta \sin \varphi \\ z = r(\vartheta, \varphi) \cos \vartheta. \end{cases} \quad (8)$$

184 The difference between the two possible choices which were presented above is  
185 shown in Fig. 4. For the case described by Eq. (6), the following parameters  
186 have been adopted:  $\vartheta_0 = \pi/6$ ,  $a = \vartheta_0^2$ ; for that represented by Eq. (7)  
187  $\vartheta_0 = \pi/6$ ,  $a = 1/50$ ,  $b = 50$ . In both cases  $g(\varphi)$  has been defined as in  
188 Eq. (5) where a value  $n = 36$  has been assumed; for comparison purposes  
189 the opening of the dome has been fixed in both cases to the value  $\vartheta_f = \pi/5$ .  
190 A magnified portion of the corrugated edge is shown for both cases in Fig. 5.

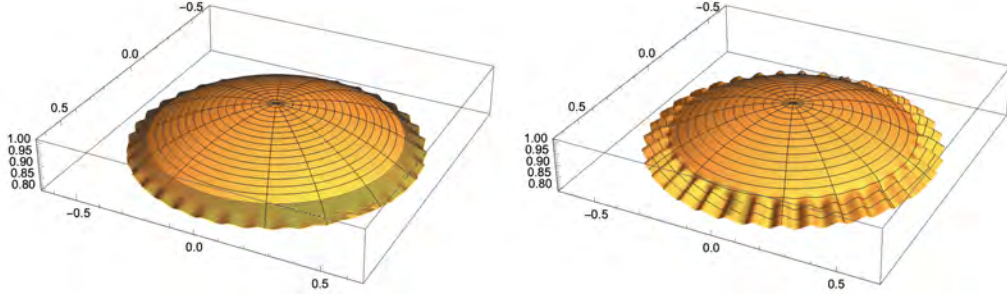


Figure 4: Corrugated surface produced by two possible choices of the perturbation function  $f(\vartheta)$ : unit step function, Eq. (6) (left) and hyperbolic tangent, Eq. (7) (right). In both cases the same opening of the dome  $\vartheta_f$  and unperturbed radius  $R_0$  have been assumed.

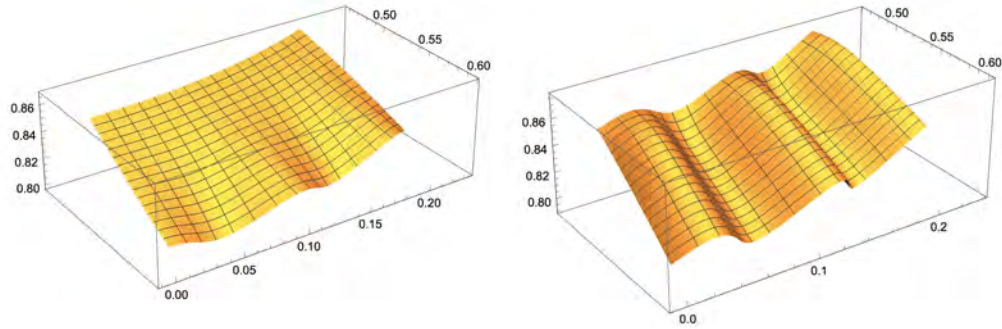


Figure 5: Magnified portion of the corrugated edge for the two cases presented in Eq. (6) (left) and Eq. (7) (right).

### 191 3. Generating a suitable geometry for FE computations

192 Starting from the above introduced parametric description of the corru-  
 193 gated shell surface, it is now possible to generate a geometry which is suitable  
 194 for the subsequent either linear or non-linear analyses. Of course to this aim,

1  
2  
3  
4  
5  
6  
7  
8  
9  
10 195 geometry formulation must be accurate. Indeed, in non-linear analyses any  
11 196 imperfection would result in a sudden reduction of the critical load. It is com-  
12  
13 197 mon to introduce slight imperfections (related to the geometry) to trigger an  
14  
15 198 equilibrium path bifurcation in large-displacement or buckling analyses [44–  
16  
17 199 48]. Now, a standard procedure to create a geometric model adopts usually  
18  
19 200 a flat-faceted surface generated by CAD software. This does not guarantee  
20  
21 201 that geometrical accuracy can be achieved in subsequent computations. A  
22  
23 202 better option consists in using computational tools such as Non Uniform Ra-  
24  
25 203 tional Basis Spline functions (henceforth, NURBS) to model the surface. To  
26  
27 204 conceive a geometric object, the following steps must be followed. As a basic  
28  
29 205 criterion, given the cyclic symmetry of the surface, only a piece of surface  
30  
31 206 must be generated, for instance (in the present case) one of the slices lying  
32  
33 207 between two subsequent supports has been drawn. In Nervi’s dome, there  
34  
35 208 are 36 supports and each such slice spans exactly  $10^\circ$ . The procedure for  
36  
37 209 generating the geometry, which is described in Fig. 6, can be summarized as  
38  
39 210 follows:

- 40  
41 211 i. A code has been developed in geometric modelling software, whose  
42  
43 212 aim is to use the parametric equation of the surface to numerically  
44  
45 213 compute a satisfactory set of coordinate pairs  $(\vartheta_i, \varphi_i)$ . The dimension  
46  
47 214 set depends on the specified number of points along the colatitude and  
48  
49 215 longitude direction. A cross-reference algorithm is employed to create  
50  
51 216 a pair  $(\vartheta_i, \varphi_i)$ , representing a single point belonging to the surface.  
52  
53 217 Therefore, a numerical algorithm (available on the software library),  
54  
55 218 employing NURBS, is applied to the points set. This allows producing a  
56  
57 219 NURBS surface using the points set as control points that will similarly

1  
2  
3  
4  
5  
6  
7  
8  
9  
10  
11  
12  
13  
14  
15  
16  
17  
18  
19  
20  
21  
22  
23  
24  
25  
26  
27  
28  
29  
30  
31  
32  
33  
34  
35  
36  
37  
38  
39  
40  
41  
42  
43  
44  
45  
46  
47  
48  
49  
50  
51  
52  
53  
54  
55  
56  
57  
58  
59  
60  
61  
62  
63  
64  
65

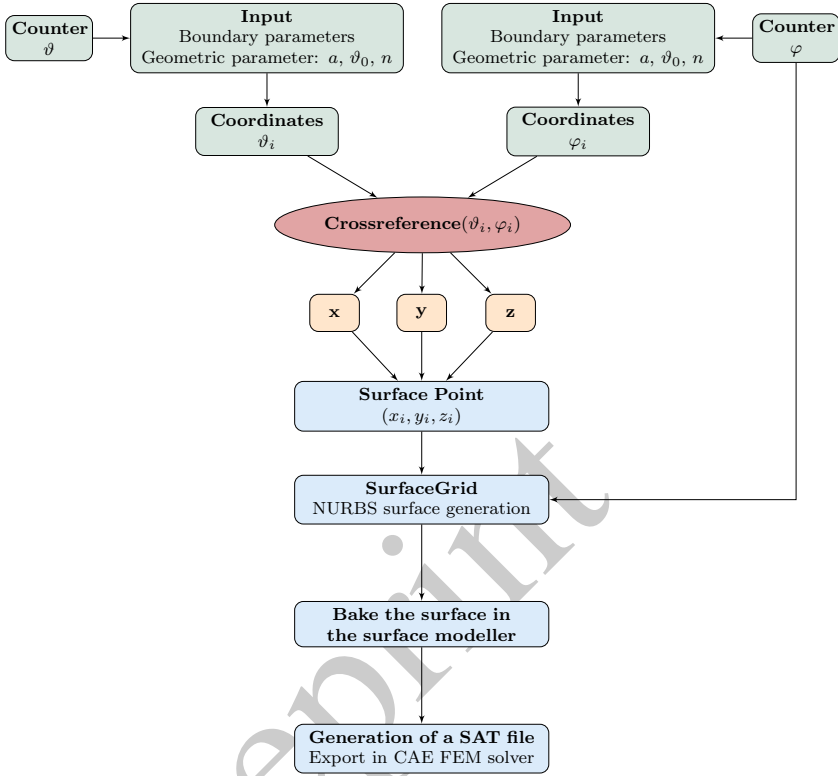


Figure 6: Block-diagram of surface generating algorithm.

- reproduce the shape. The accuracy of the representation depends on the initial user choice. Nevertheless, it is clear that the accuracy in generating the surface depends on the chosen number of points;
- ii. The algorithm outcome is then graphically visualized in the surface modeler. To produce the obtained NURBS surface, it is necessary to bake it into the graphical interface;
  - iii. The surface is exported into a convenient file exchange format, such as the ACIS format. This file includes complete pieces of information

1  
2  
3  
4  
5  
6  
7  
8  
9  
10  
11  
12  
13  
14  
15  
16  
17  
18  
19  
20  
21  
22  
23  
24  
25  
26  
27  
28  
29  
30  
31  
32  
33  
34  
35  
36  
37  
38  
39  
40  
41  
42  
43  
44  
45  
46  
47  
48  
49  
50  
51  
52  
53  
54  
55  
56  
57  
58  
59  
60  
61  
62  
63  
64  
65

228 about the geometry and can be imported into an advanced FEM solver;  
229 iv. The ACIS file is imported into the CAE FEM solver and constitutes a  
230 single portion of the surface, see Fig. 7. Inside the pre-processor, the  
231 portion is suitably reflected and then a circular pattern is implemented  
232 around the  $z$ -axis to generate the whole dome. All these slices need  
233 then to be merged into a single object.

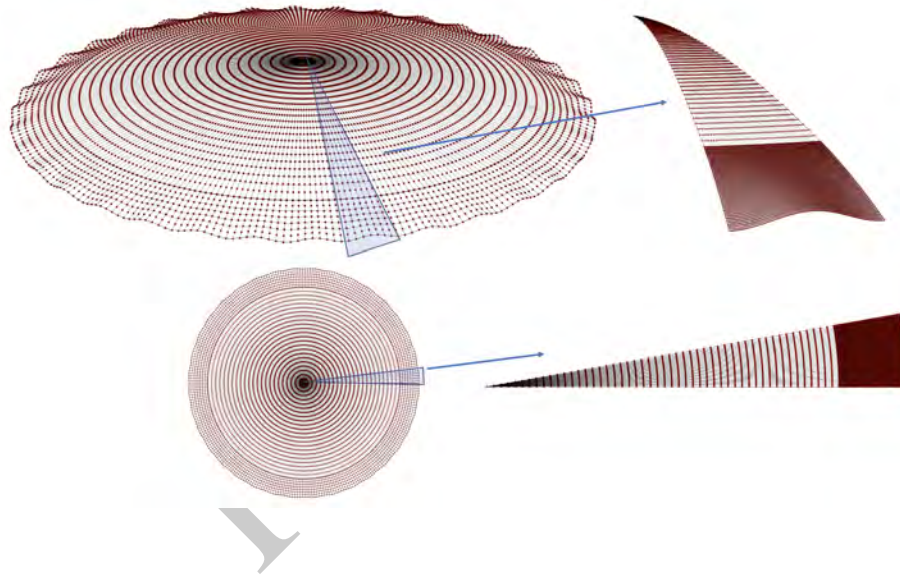
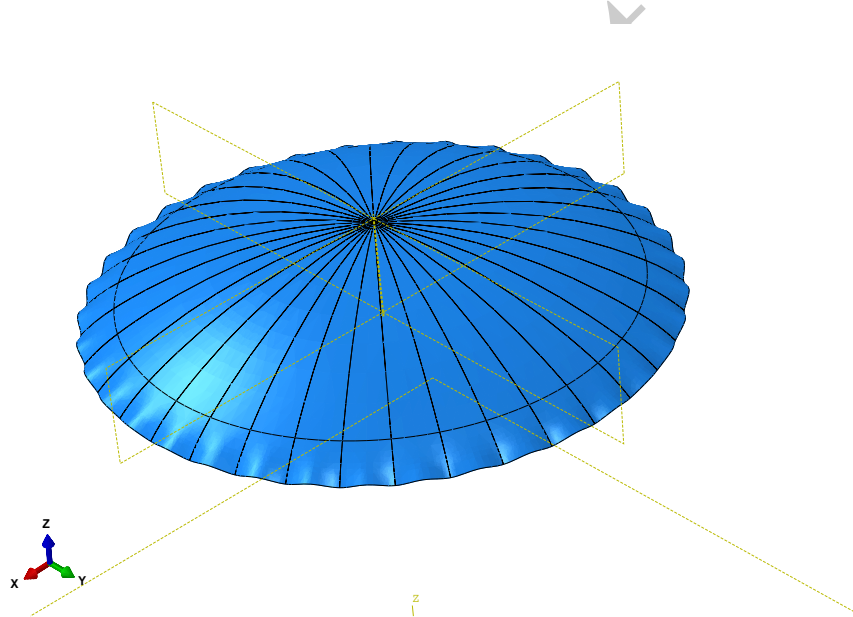


Figure 7: The automatically generated set of points for the model of Nervi's dome of Palasport Flaminio.

234 The obtained part can then be meshed inside the FE pre-processor. It is  
235 requested that even the mesh closely reproduces the shape without deforming  
236 the geometry. As a consequence, the chosen type of finite element should be  
237 able to reproduce a conveniently small portion of double-curvature surface  
238 such as an eight-noded shell element with six or five degrees of freedom, and  
239 where that is not possible (e.g. in the dome apex) to six-noded triangular



1  
2  
3  
4  
5  
6  
7  
8  
9  
240 elements with five degrees of freedom. In addition, this kind of elements is  
10  
241 suitable to perform buckling analysis. However, to obtain a regular mesh,  
11  
12  
242 a sweep algorithm has been used for getting a mesh made of quadrilateral  
13  
14  
243 elements, whose edges are aligned with meridians and parallels. The resulting  
15  
16  
244 mesh shows however a main drawback: indeed, the elements which are close  
17  
18  
245 to the vertex turn out to be severely distorted. In order to overcome such  
19  
20  
246 problem, a minute partition is applied near the apex. Hence, in this region  
21  
22  
247 a single six-noded triangular element is employed for each slice.



24  
25  
26  
27  
28  
29  
30  
31  
32  
33  
34  
35  
36  
37  
38  
39  
40  
41  
42  
43  
44  
45  
46  
47 Figure 8: Resulting assembly of the slices of the model of Palasport Flaminio dome.

48  
49  
50  
51  
52 **4. Geometrical and mechanical data**

53  
54  
249 The analysis of a shell inspired by RC Palasport Flaminio dome designed  
55  
56  
250 by Nervi has been accomplished. In this section the geometrical and mechan-

Table 1: Geometric properties of the Palasport Flaminio dome

Radius	$R_0$	51.039 m
Roof span	$L$	60.000 m
Shell thickness	$t$	0.200 m
Opening angle	$\vartheta_f$	$\pi/5$ rad
Angle where perturbation starts	$\vartheta_0$	$\pi/6$ rad
Wave number	$n$	36

ical assumptions adopted for such RC shell are summarized. Original design blueprints are available in the MAXXI (the Art Museum of the XXI century) archives in Rome. Besides, the span and the opening angle are given in [18], as reliable average measurements. All these data are presented in Table 1. In [49] a different opening angle has been considered, which, however, does not seem to agree with the architectural blueprints reported in [18]. Instead mechanical characterization of the material has been simplified as follows:

- i. Only the linear part of the stress-strain curve is taken into account. So, plasticity and other kind of non-linear behaviour have been disregarded;
- ii. RC is always assumed to be uncracked;
- iii. Fluage and creep are neglected, and Young's modulus  $E$  is assumed to be constant and equal to 30 GPa;
- iv. Poisson's coefficient  $\nu$  is similarly assumed to be constant and equal to

1  
2  
3  
4  
5  
6  
7  
8  
9 264 0.2;

10  
11 265 v. Concrete strength class is required to be C20/C25 (Eurocode classi-  
12 266 fication), whose density is  $2500 \text{ kg/m}^3$ . Even though Nervi's dome  
13 267 is a RC shell with stiffeners, which follow a certain spherical path, it  
14 268 is reasonable to assume that shell thickness is constant and equal to  
15 269 0.2 m.

20  
21  
22 270 For a more accurate survey about mechanical properties of concrete, partially  
23 271 based on tested specimens and survey, even though they are referred to a  
24 272 nearby canopy which was realised by the same Nervi (Stadium Flaminio) a  
25 273 reader may rely on [50].

26  
27  
28 274 In the mentioned reference, particular emphasis has been placed on the  
29 275 differences between *ferrocemento*, the building material adopted by Nervi,  
30 276 and the standard RC.

## 31 32 33 34 35 36 37 277 **5. Analysis**

38  
39  
40 278 It is now possible to carry out a statical analysis of the structure by using  
41 279 computational methods. For the sake of simplicity, only the shape produced  
42 280 by Eqs. (4), (5) and (6) has been considered.

43  
44  
45 281 The load-case consists of a uniform external normal pressure  $q_0$  applied  
46 282 inwards to the whole surface, whose magnitude is 5 kPa. To understand  
47 283 the effect of edge-corrugation, a comparison between a shell with the same  
48 284 geometrical measure but without corrugation is shown.

49  
50  
51 285 The structure has been envisioned to behave according to the classical  
52 286 membrane theory. In agreement with this theory, supports should restrain

287 motion only along the tangent direction. According to that, the dome edge re-  
 288 quires to be simply supported, so that edge rotation and out-of-plane surface  
 289 extension/shrinking are allowed. Therefore, the designer put all his efforts  
 290 to guarantee that no edge disturbances occur. As a matter of fact, the pillar  
 291 inclination follows the tangent to the boundary surface. Nevertheless, the  
 292 edge is fully restrained on the support and free between the supports. If  
 293 other constraints are applied, the membrane state will be supplemented by  
 294 bending and twisting effects. As a consequence, such supplementary effects  
 295 should be taken into account.

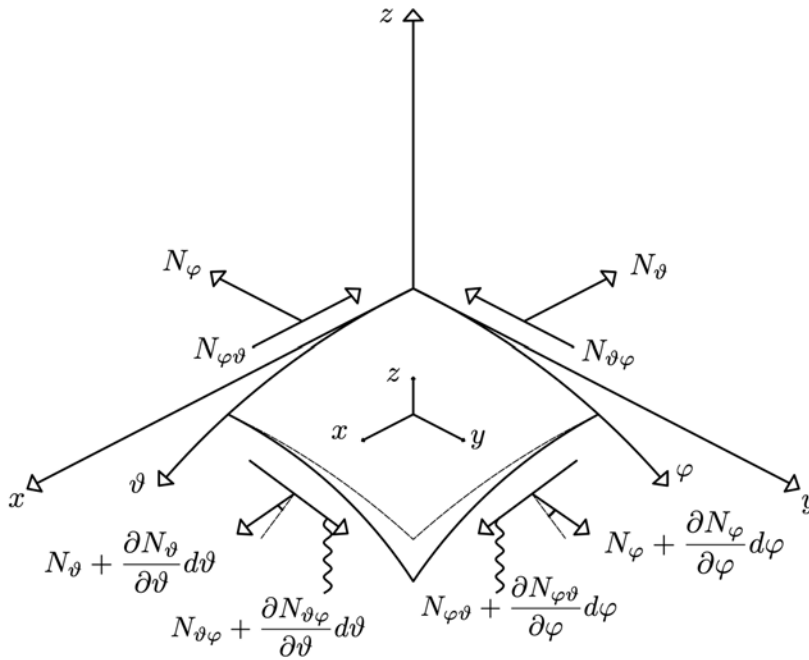


Figure 9: Equilibrium of a differential element of a shell with membrane stress-resultants.

296 In terms of the membrane stress resultants  $N_\vartheta$ ,  $N_\varphi$  and  $N_{\vartheta\varphi} = N_{\varphi\vartheta}$ , which

1  
2  
3  
4  
5  
6  
7  
8  
9  
297 are, respectively, the in-plane normal components of stress directed along the  
10  
298 meridian line and the parallel line, and the in plane shear stress components  
11  
12  
13 299 (see Fig. 9), the fundamental differential equations of equilibrium in the  
14  
15 300 membrane theory of shells, written with reference to the lines of curvature  
16  
17 301 on the middle-surface are given by [51] and read:

$$\begin{aligned}
 \frac{\partial}{\partial \vartheta}(BN_{\vartheta}) - \frac{\partial B}{\partial \vartheta}N_{\varphi} + \frac{1}{A} \frac{\partial}{\partial \varphi}(A^2N_{\vartheta\varphi}) + ABX &= 0 \\
 \frac{\partial}{\partial \varphi}(AN_{\varphi}) - \frac{\partial A}{\partial \varphi}N_{\vartheta} + \frac{1}{B} \frac{\partial}{\partial \vartheta}(B^2N_{\vartheta\varphi}) + ABY &= 0 \\
 \frac{N_{\vartheta}}{R_1} + \frac{N_{\varphi}}{R_2} - Z &= 0.
 \end{aligned} \tag{9}$$

29 In Eq. (9)  $A$  and  $B$  are the coefficients of the first fundamental form, which  
30  
31 303 gives the squared length of a line element as:

$$ds^2 = A^2d\vartheta^2 + B^2d\varphi^2;$$

304  $R_1$  and  $R_2$  are, respectively, the curvature radii along the meridian ( $\vartheta$ -line)  
35  
36  
37  
38 305 and perpendicularly to it;  $X$  and  $Y$  are external surface loads (i.e. loads per  
39  
40 306 unit area) acting towards increasing values of  $\vartheta$  and  $\varphi$ , while  $Z$  denotes the  
41  
42 307 intensity of surface load per unit area acting along the outward normal.

43  
44  
45 308 So, for a perfectly spherical shell, whose radius is  $R_0$ , acted upon by  
46  
47 309 a constant external, inward-directed pressure  $q_0$ , the previous equations do  
48  
49 310 simplify because  $R_1 = R_0$ ,  $R_2 = R_0$ ,  $A = R_0$ ,  $B = R_0 \sin \vartheta$ ; moreover  $X = 0$ ,  
50  
51 311  $Y = 0$ ,  $Z = -q_0$ . Finally for the axial symmetry, it is everywhere  $N_{\vartheta\varphi} = 0$   
52  
53 312 and  $N_{\vartheta} = N_{\vartheta}(\vartheta)$ ,  $N_{\varphi} = N_{\varphi}(\vartheta)$ , i.e. they do depend only on colatitude.

54  
55 313 The reference solution for a membrane state produced by a uniform pres-  
56  
57 314 sure load  $q_0$  acting on a hemispherical shell supported along the equator is

1  
2  
3  
4  
5  
6  
7  
8  
9  
315 well-known and can be found, if attention is restricted to some of the major  
10  
316 sources only, in [52–54]. Indeed it results:

13  
14  
15  
16  
317 
$$N_{\vartheta} = N_{\varphi} = -q_0 \frac{R_0}{2} \quad (10)$$

17  
18  
19  
20  
21  
22  
23  
24  
25  
26  
27  
28  
29  
30  
31  
32  
318 It should be emphasized that  $N_{\vartheta}$  and  $N_{\varphi}$ , which are given by Eq. (10) and  
319 will be used in the sequel as a measure of variance from a perfect membrane  
320 state, represent the resultant of the corresponding local stress components  
321  $\sigma_{\vartheta}$ ,  $\sigma_{\varphi}$ , once they are integrated along the thickness of the shell,  $t$ . Important,  
322 both theoretical and experimental references about RC shells behaviour can  
323 be found in [55–57]. On the other hand, a theoretical solution in terms  
324 of Fourier series for a hemispherical shells on discrete supports was set out  
325 in [52, 56].

32  
33  
34  
35  
36  
37  
38  
39  
40  
41  
326 The numerical solutions for the edge-corrugated spherical shells produce local  
327 surface stresses, whose general expressions can be computed in terms of the  
328 section resultants  $N_{\vartheta}$  and  $N_{\varphi}$  as

39  
40  
41  
42  
43  
44  
45  
46  
47  
48  
49  
50  
51  
52  
53  
54  
55  
56  
57  
58  
59  
60  
61  
62  
63  
64  
65  
$$\sigma_{\vartheta} = \frac{N_{\vartheta}}{t}, \quad \sigma_{\varphi} = \frac{N_{\varphi}}{t}.$$

329 In particular,  $\sigma_{\vartheta}$  is the normal stress acting along the  $\vartheta$  direction (i.e. that  
330 tangent to the meridian) and  $\sigma_{\varphi}$  is the normal stress along the  $\varphi$  direction,  
331 namely tangent to the parallel.

332 It should be noticed that, even for the corrugated shell, the above men-  
333 tioned directions are principal direction of stress for the considered applied  
334 load, namely uniform external pressure. All numerical results related to stress  
335 are presented in dimensionless form: stress values are indeed divided by the  
336 applied external pressure  $q_0 = 5$  kPa, while the angular position is given in

1  
2  
3  
4  
5  
6  
7  
8  
9  
10  
11  
12  
13  
14  
15  
16  
17  
18  
19  
20  
21  
22  
23  
24  
25  
26  
27  
28  
29  
30  
31  
32  
33  
34  
35  
36  
37  
38  
39  
40  
41  
42  
43  
44  
45  
46  
47  
48  
49  
50  
51  
52  
53  
54  
55  
56  
57  
58  
59  
60  
61  
62  
63  
64  
65

337 the dimensionless form  $\vartheta/\vartheta_f$ , where  $\vartheta_f$  is the colatitude value corresponding  
338 to the position of the edge, which is assumed to be the same in all considered  
339 cases.

340 The stresses  $\sigma_\vartheta$  and  $\sigma_\varphi$  along the shell are displayed in the contour plot  
341 on the left of Fig. 10 and Fig. 11.

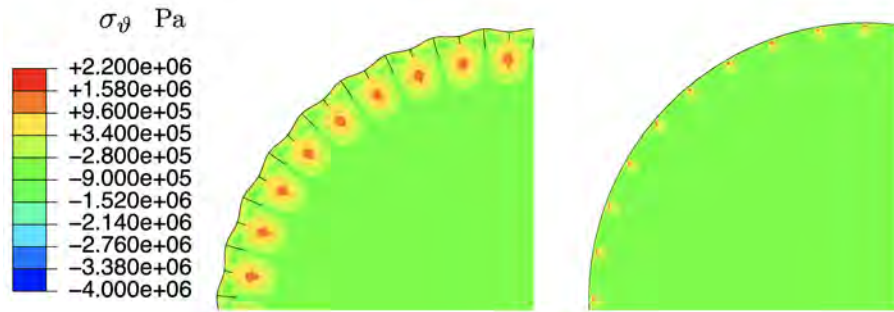


Figure 10: Contour plot of the stress component  $\sigma_\vartheta$  for the corrugated-edge dome (left) and for the spherical cap without corrugation (right). In both cases, 36 discrete supports have been considered.

342 As it is expected, the solution exhibits cyclic symmetry. A comparison with  
343 a non-corrugated shell is displayed on the right of Fig. 10 and of Fig. 11.

344 The stresses corresponding to two meridians, one passing through a support  
345 and the other through the crest of a wave will be considered in detail; the  
346 output is concisely shown in the graphs that follow.

347 In particular, Fig. 12 and Fig. 13 show on the left  $\sigma_\vartheta$  for the above mentioned  
348 meridians, while the stress component  $\sigma_\varphi$  is shown, for the same meridians,  
349 on the right of the above mentioned Figures.

350 To understand the reason why in the corrugated shell there is a reduction  
351 of stresses, one can usefully look at the bending moment diagrams. Let

1  
2  
3  
4  
5  
6  
7  
8  
9  
10  
11  
12  
13  
14  
15  
16  
17  
18  
19  
20  
21  
22  
23  
24  
25  
26  
27  
28  
29  
30  
31  
32  
33  
34  
35  
36  
37  
38  
39  
40  
41  
42  
43  
44  
45  
46  
47  
48  
49  
50  
51  
52  
53  
54  
55  
56  
57  
58  
59  
60  
61  
62  
63  
64  
65

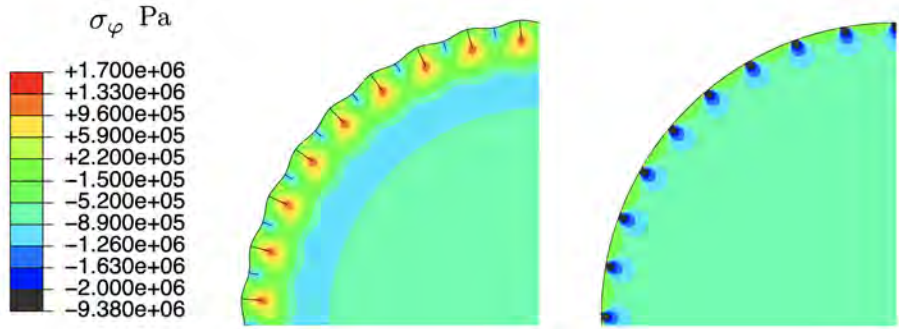


Figure 11: Contour plot of the stress component  $\sigma_\varphi$  for the corrugated-edge dome (left) and for the spherical cap without corrugation (right). In both cases, 36 discrete supports have been considered.

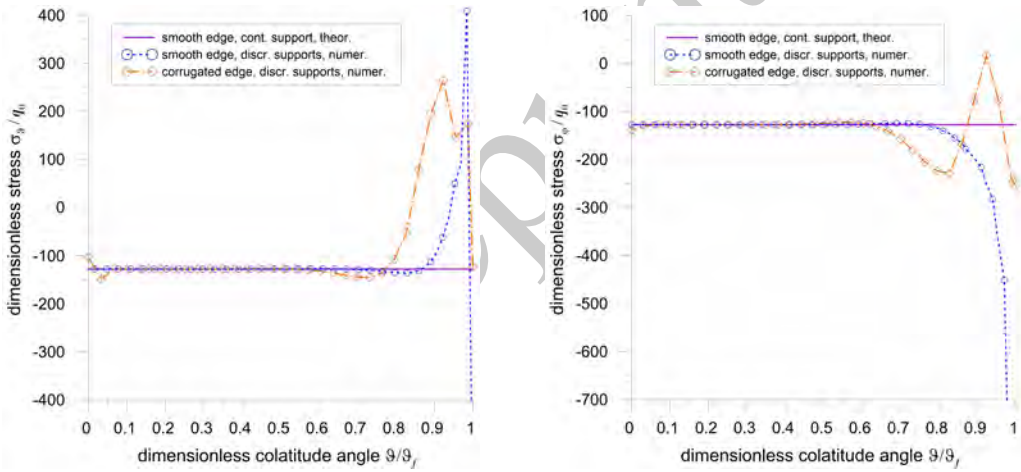


Figure 12: Stress components  $\sigma_\theta$  and  $\sigma_\varphi$  along a meridian passing through a support.

352  $M_\theta$  be the section moment (which is dimensionally expressed as the ratio  
 353 moment/thickness, thus being homogeneous to a force) along the  $\theta$  direction  
 354 and  $M_\varphi$  the section moment along the  $\varphi$  direction. Fig. 14 shows the contour  
 355 plot of the section moment  $M_\theta$  for an edge-corrugated (left) and for a non  
 356 corrugated shell (right).

357 Similarly, Fig. 15 shows the contour plot of the section moment  $M_\varphi$  for an



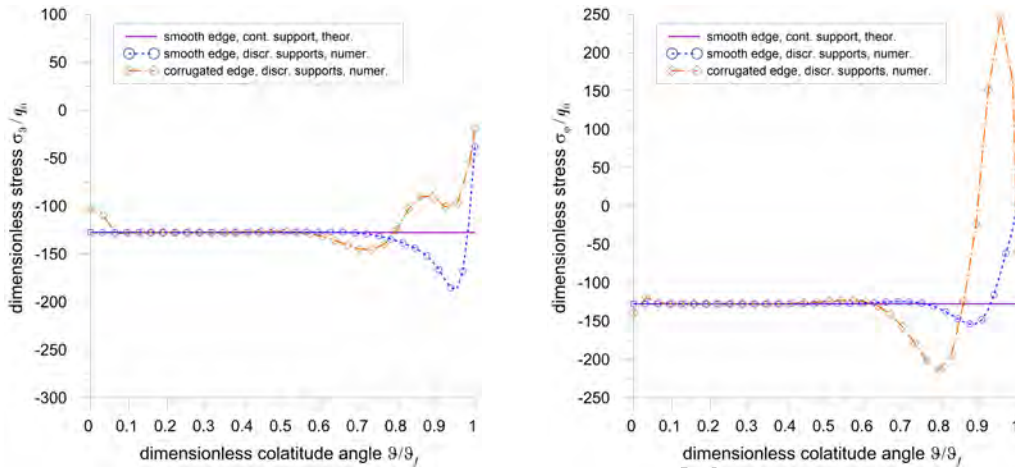


Figure 13: Stress components  $\sigma_\theta$  and  $\sigma_\varphi$  along a meridian located between two supports, i.e. corresponding to the crest of the wave.

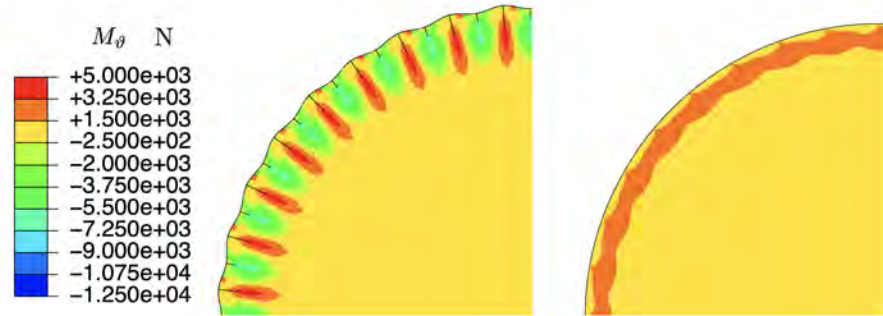


Figure 14: Contour plot of the section moment,  $M_\theta$  for the corrugated-edge dome (left) and for the spherical cap without corrugation (right). In both cases 36 discrete supports have been considered.

edge-corrugated (left) and for a non corrugated shell (right).

The section moments have been plotted for two different meridians, one passing through a support, the other through the crest of the wave. The output is shown in Fig. 16 and 17 in dimensionless form, by dividing the relevant values by the constant  $M_0 = 5000$  kN.

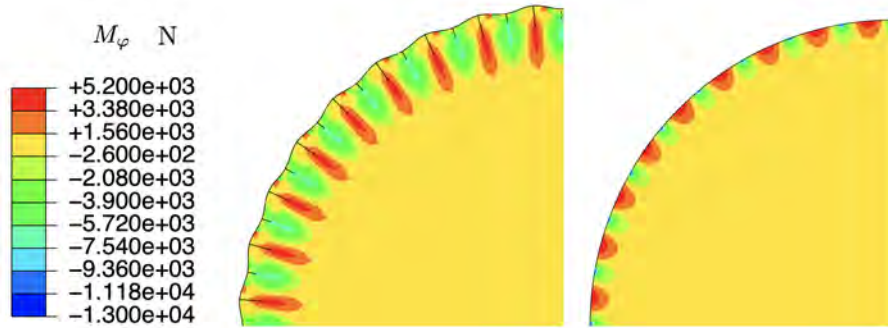


Figure 15: Contour plot of the section moment  $M_\varphi$  for the corrugated-edge dome (left) and for the spherical cap without corrugation (right). In both cases 36 discrete supports have been considered.

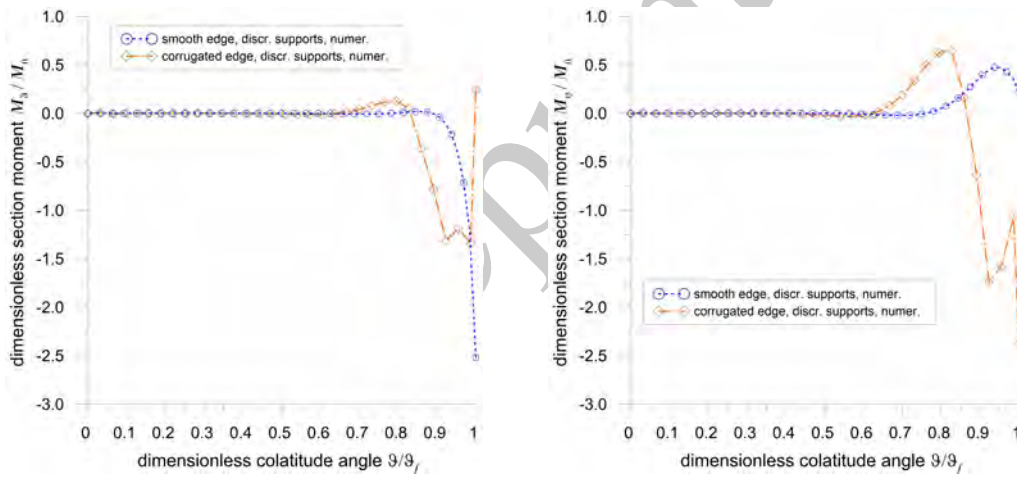


Figure 16: Section moments  $M_\theta$  and  $M_\varphi$  along a meridian passing through a support.

363  $M_\theta$  (left) and  $M_\varphi$  (right) are plotted in Fig. 16 with reference to the meridian  
 364 passing through one of the supports; instead the same section moments, in  
 365 the same order, are plotted in Fig. 17 for a meridian which passes through  
 366 the crest of the corrugation.

367 It can be pointed out the meaningful decrease, along the meridian direction,  
 368 of the bending moment in the corrugated shell, in comparison with the non-

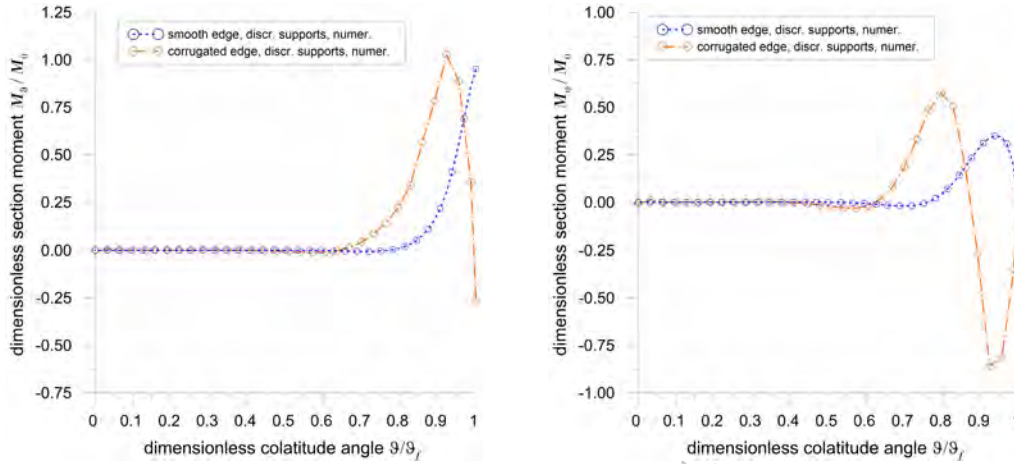


Figure 17: Section moments  $M_\vartheta$  (left) and  $M_\varphi$  (right) along a meridian located between two supports, i.e. corresponding to the crest of the wave.

369 corrugated one. That is the most relevant issue. Indeed corrugation, due  
 370 to its shape, allows for a significant reduction of the bending moment: close  
 371 to the edge  $M_\vartheta$  exhibits a noteworthy reduction involving even an inversion  
 372 of its signum. This improvement can be clearly perceived as a consequence  
 373 of the increment of the section inertia of the shell. On the other hand,  
 374  $M_\varphi$  is not similarly subjected to a significant decrease since the surface is  
 375 essentially warped in the  $\varphi$  direction. Nonetheless, from the point of view of  
 376 the designer, this difference of behaviour in terms of bending moments has  
 377 little significance, since for RC shells the standard design rules suggest to  
 378 adopt symmetric steel bar reinforcement along both  $\vartheta$  and  $\varphi$  directions.

## 379 6. Conclusion

380 The parametric equations for a shell whose edge is corrugated have been  
 381 proposed and a suitable FE simulation procedure, which accurately handles

1  
2  
3  
4  
5  
6  
7  
8  
9 382 the doubly curved geometry, has been presented.

10  
11 383 It has been shown through numerical simulation what was intuitively  
12  
13 384 clear to P.L. Nervi: a corrugation along the edge enhances the structural  
14  
15 385 performance of a shell. Furthermore, corrugation considerably decreases the  
16  
17 386 bending moment produced by discrete supports along the shell edge. Indeed,  
18  
19 387 although the shell is designed to behave as a perfect membrane, it can be  
20  
21 388 affected by significant bending on its edge. A reliable procedure has been  
22  
23 389 introduced to study the influence of corrugation into the above-mentioned  
24  
25 390 structures and to evaluate their stress distribution.

26  
27 391 The original architectural function related to P.L. Nervi's work, which  
28  
29 392 represents the inspiration for the present paper, has been developed in the  
30  
31 393 sense of Civil and Structural Engineering: corrugated shell structures can be  
32  
33 394 both simply used as a canopy endowed also with some aesthetics, and can  
34  
35 395 be introduced in buildings for their high-performance mechanical properties,  
36  
37 396 like in the case of roofs for special and nuclear waste containers. In this case,  
38  
39 397 a unique shallow shell element must cover the vessel.

40  
41 398 Other applications can be found in the field of automatization of build-  
42  
43 399 ing processes. The procedure, which has been presented in this paper, may  
44  
45 400 be applied to different shapes, such as free-form shells and concrete printed  
46  
47 401 structures. Some advancements could be related in the LIDAR field and  
48  
49 402 to accurately identify the influence of small deviation in the structural be-  
50  
51 403 haviour, a comparison between a theoretical shape and *in situ* surveys could  
52  
53 404 be done. A main issue, which is related to the topic discussed in the present  
54  
55 405 work, will be developed in the following investigations and involves the role  
56  
57 406 of corrugation in instability phenomena, such as snap-through. It constitutes

1  
2  
3  
4  
5  
6  
7  
8  
9  
10  
11  
12  
13  
14  
15  
16  
17  
18  
19  
20  
21  
22  
23  
24  
25  
26  
27  
28  
29  
30  
31  
32  
33  
34  
35  
36  
37  
38  
39  
40  
41  
42  
43  
44  
45  
46  
47  
48  
49  
50  
51  
52  
53  
54  
55  
56  
57  
58  
59  
60  
61  
62  
63  
64  
65

indeed a very challenging problem, whose solution has not been achieved yet.

The methods developed in this paper for Civil Engineering and Architecture applications can be simply generalized to be used in different scientific milieux. One can, for example, use them in the field of Bioengineering for designing new smart contact lenses. This will be the topic of a future development. Moreover, the presented study can be completed and enhanced by taking into account results originally developed for the so-called generalized theories: many interesting phenomena may arise if one introduces higher gradient models like in [58–62].

Numerics play a fundamental role in the solution of problems like that presented in this article: different numerical methods can help in studying different phenomena and they could be implemented also in the study of corrugated shells. One might refer to [63–68] for a detailed discussion.

## 7. Declaration of competing interest

The authors declare that they have no known competing financial interests or personal relationships that could have appeared to influence the work reported in this paper.

## 8. Acknowledgements

The authors are grateful to Ph.D. Daniel Meloni for his valuable advice about the use of FE software. The authors are grateful to Prof. Victor Eremeyev for the fruitful discussions.

This research has been developed for the partial fulfillment of the doctoral program of M. Lai at *Scuola di dottorato in Ingegneria Civile e Architettura*,

1  
2  
3  
4  
5  
6  
7  
8  
9 430 *University of Cagliari*. It was also carried out under the financial grant  
10  
11 431 of *Place-Doc Exchange Agreement* between the University of Cagliari and  
12  
13 432 the University of Stuttgart, Institute for Non-linear Mechanics, under the  
14  
15 433 supervision of S. Eugster.

16  
17 434 The financial support of Fondazione di Sardegna through grant *Surveying,*  
18  
19 435 *modelling, monitoring and rehabilitation of masonry vaults and domes* i.e.  
20  
21 436 *Rilievo, modellazione, monitoraggio e risanamento di volte e cupole in mu-*  
22  
23 437 *ratura (RMMR)* (CUP code: F72F20000320007) is grateful acknowledged by  
24  
25 438 M. Lai, E. Reccia, A. Cazzani.

26  
27 439 M. Spagnuolo was supported by P.O.R. Sardegna F.S.E. 2014–2020 *Asse*  
28  
29 440 *III: Istruzione e Formazione, Obiettivo Tematico: 10, Obiettivo Specifico:*  
30  
31 441 *10.5, Azione dell'accordo di Partenariato:10.5.12 — Avviso di chiamata per*  
32  
33 442 *il finanziamento di Progetti di ricerca, Anno 2017*; this support is gratefully  
34  
35 443 acknowledged, too.

## 37 444 **References**

- 38  
39  
40 445 [1] J. O'Neill, "Walls in half-circles and serpentine walls", *Garden History*,  
41  
42 446 vol. 8, no. 3, pp. 69–76, 1980.
- 43  
44  
45 447 [2] I. Giorgio, U. Andreaus, and A. Madeo, "The influence of different loads  
46  
47 448 on the remodeling process of a bone and bioresorbable material mixture  
48  
49 449 with voids", *Continuum Mechanics and Thermodynamics*, vol. 28, no. 1-  
50  
51 450 2, pp. 21–40, 2016.
- 52  
53  
54 451 [3] I. Giorgio, F. dell'Isola, U. Andreaus, F. Alzahrani, T. Hayat, and  
55  
56 452 T. Lekszycki, "On mechanically driven biological stimulus for bone re-

1  
2  
3  
4  
5  
6  
7  
8  
9  
10  
11  
12  
13  
14  
15  
16  
17  
18  
19  
20  
21  
22  
23  
24  
25  
26  
27  
28  
29  
30  
31  
32  
33  
34  
35  
36  
37  
38  
39  
40  
41  
42  
43  
44  
45  
46  
47  
48  
49  
50  
51  
52  
53  
54  
55  
56  
57  
58  
59  
60  
61  
62  
63  
64  
65

453 modeling as a diffusive phenomenon”, *Biomechanics and Modeling in*  
454 *Mechanobiology*, vol. 18, no. 6, pp. 1639–1663, 2019.

455 [4] Y. Lu and T. Lekszycki, “New description of gradual substitution of graft  
456 by bone tissue including biomechanical and structural effects, nutrients  
457 supply and consumption”, *Continuum Mechanics and Thermodynamics*,  
458 vol. 30, no. 5, pp. 995–1009, 2018.

459 [5] B. Desmorat and R. Desmorat, “Topology optimization in damage gov-  
460 erned low cycle fatigue”, *Comptes Rendus Mecanique*, vol. 336, no. 5,  
461 pp. 448–453, 2008.

462 [6] I. Giorgio and D. Scerrato, “Multi-scale concrete model with rate-  
463 dependent internal friction”, *European Journal of Environmental and*  
464 *Civil Engineering*, vol. 21, no. 7-8, pp. 821–839, 2017.

465 [7] D. Scerrato, I. Giorgio, A. Madeo, A. Limam, and F. Darve, “A simple  
466 non-linear model for internal friction in modified concrete”, *International*  
467 *Journal of Engineering Science*, vol. 80, pp. 136–152, 2014.

468 [8] D. Scerrato, I. Giorgio, A. della Corte, A. Madeo, N. Dowling, and  
469 F. Darve, “Towards the design of an enriched concrete with enhanced dis-  
470 sipation performances”, *Cement and Concrete Research*, vol. 84, pp. 48–  
471 61, 2016.

472 [9] F. Stochino, M. L. Fadda, and F. Mistretta, “Low cost condition assess-  
473 ment method for existing RC bridges”, *Engineering Failure Analysis*,  
474 vol. 86, pp. 56–71, 2018.

- 1  
2  
3  
4  
5  
6  
7  
8  
9  
10 475 [10] M. Coni, F. Mistretta, F. Stochino, J. Rombi, M. Sassu, and M. L. Pup-  
11 476 pio, “Fast falling weight deflectometer method for condition assessment  
12  
13 477 of RC bridges”, *Applied Sciences*, vol. 11, no. 4, p. 1743, 2021.
- 14  
15  
16 478 [11] F. Mistretta, G. Sanna, F. Stochino, and G. Vacca, “Structure from  
17  
18 479 motion point clouds for structural monitoring”, *Remote Sensing*, vol. 11,  
19  
20 480 no. 16, p. 1940, 2019.
- 21  
22  
23 481 [12] F. Stochino and F. Lopez Gayarre, “Reinforced concrete slab optimiza-  
24  
25 482 tion with simulated annealing”, *Applied Sciences*, vol. 9, no. 15, p. 3161,  
26  
27 483 2019.
- 28  
29 484 [13] E. Torroja, “Razón y ser de los tipos estructurales”, tech. rep., Con-  
30  
31 485 sejo Superior de Investigaciones Científicas, Instituto de Ciencias de la  
32  
33 486 Construcción "Eduardo Torroja", Madrid, 2000.
- 34  
35  
36 487 [14] C. Siegel, *Struttura e forma dell'architettura moderna*. Bologna: CELI,  
37  
38 488 1968.
- 39  
40  
41 489 [15] G. Pizzetti and A. M. Zorno Trisciuoglio, *Principi statici e forme strut-*  
42  
43 490 *turali*. Torino: Utet, 1980.
- 44  
45 491 [16] T. Iori and S. Poretti, *SIXXI. Storia dell'ingegneria strutturale in Italia*,  
46  
47 492 vol. 1-5. Roma: Gangemi, 2014.
- 48  
49  
50 493 [17] P. L. Nervi, G. Neri, M. A. Chiorino, and A. Rossi, *Scienza o arte del*  
51  
52 494 *costruire?: Caratteristiche e possibilità del cemento armato*. Milano:  
53  
54 495 CittàStudi, 2014.



- 1  
2  
3  
4  
5  
6  
7  
8  
9  
10 496 [18] P. Solomita, *Pier Luigi Nervi vaulted architecture: towards new struc-*  
11 497 *tures*. Bologna: Bononia University Press, 2015.
- 12  
13  
14 498 [19] T. Leslie, “Carpenter’s parametrics: economics, efficiency, and form in  
15 499 Pier Luigi Nervi’s concrete designs”, *Journal of the International Asso-*  
16 *ciation for Shell and Spatial Structures*, vol. 54, no. 2-3, pp. 107–115,  
17 500 2013.  
18  
19  
20  
21  
22 502 [20] E. Tomei, “The Iris Dome”, *L’Arca*, vol. 73, pp. 55–57, 1993.
- 23  
24  
25 503 [21] C. A. B. Hyeng and S. N. Krivoshapko, “Umbrella-type surfaces in ar-  
26 504 chitecture of spatial structures”, *IOSR Journal of Engineering*, vol. 3,  
27 505 no. 3, pp. 43–53, 2013.
- 28  
29  
30  
31  
32 506 [22] S. N. Krivoshapko and V. N. Ivanov, *Encyclopedia of analytical surfaces*.  
33 507 Cham: Springer, 2015.
- 34  
35  
36 508 [23] S. Malek and C. Williams, “The equilibrium of corrugated plates and  
37 509 shells”, *Nexus Network Journal*, vol. 19, no. 3, pp. 619–627, 2017. ISBN:  
38 510 1522-4600 Publisher: Springer.
- 39  
40  
41  
42  
43 511 [24] A. Norman, S. Guest, and K. Seffen, “Novel multistable corrugated  
44 512 structures”, in *48th AIAA/ASME/ASCE/AHS/ASC Structures, Struc-*  
45 513 *tural Dynamics, and Materials Conference*, p. 2228, 2007.
- 46  
47  
48  
49  
50 514 [25] T. Michiels, S. Adriaenssens, and M. Dejong, “Form finding of corru-  
51 515 gated shell structures for seismic design and validation using non-linear  
52 516 pushover analysis”, *Engineering Structures*, vol. 181, pp. 362–373, 2019.
- 53  
54  
55  
56  
57  
58  
59  
60  
61  
62  
63  
64  
65

- 1  
2  
3  
4  
5  
6  
7  
8  
9  
517 [26] H. Altenbach and V. A. Eremeyev, *Shell-like structures: Non-classical*  
10 *theories and applications*. Berlin: Springer, 2011.  
11  
12  
13  
14 [27] H. Altenbach and V. A. Eremeyev, “On the shell theory on the nanoscale  
15 with surface stresses”, *International Journal of Engineering Science*,  
16 vol. 49, no. 12, pp. 1294–1301, 2011.  
17  
18  
19  
20 [28] J. Altenbach, H. Altenbach, and V. A. Eremeyev, “On generalized  
21 Cosserat-type theories of plates and shells: a short review and bibli-  
22 ography”, *Archive of Applied Mechanics*, vol. 80, no. 1, pp. 73–92, 2010.  
23  
24 [29] V. A. Eremeyev, “Two- and three-dimensional elastic networks with rigid  
25 junctions: modeling within the theory of micropolar shells and solids”,  
26 *Acta Mechanica*, vol. 230, no. 11, pp. 3875–3887, 2019.  
27  
28  
29  
30 [30] V. Eremeyev and H. Altenbach, “Basics of mechanics of micropolar  
31 shells”, in *Shell-like Structures* (H. Altenbach and V. Eremeyev, eds.),  
32 vol. 572, pp. 63–111, Cham: Springer, 2017.  
33  
34  
35  
36 [31] J. Chróscielewski, F. dell’Isola, V. A. Eremeyev, and A. Sabik, “On  
37 rotational instability within the nonlinear six-parameter shell theory”,  
38 *International Journal of Solids and Structures*, vol. 196-197, pp. 179–  
39 189, 2020.  
40  
41  
42  
43 [32] V. A. Eremeyev, “A nonlinear model of a mesh shell”, *Mechanics of*  
44 *Solids*, vol. 53, no. 4, pp. 464–469, 2018.  
45  
46  
47  
48 [33] A. M. Bersani, I. Giorgio, and G. Tomassetti, “Buckling of an elastic  
49 hemispherical shell with an obstacle”, *Continuum Mechanics and Ther-*  
50 *modynamics*, vol. 25, no. 2-4, pp. 443–467, 2013.  
51  
52  
53  
54  
55  
56  
57  
58  
59  
60  
61  
62  
63  
64  
65

- 1  
2  
3  
4  
5  
6  
7  
8  
9  
10 540 [34] L. Greco and M. Cuomo, “An implicit  $G^1$ -conforming bi-cubic interpo-  
11 541 lation for the analysis of smooth and folded Kirchhoff–Love shell as-  
12 542 semblies”, *Computer Methods in Applied Mechanics and Engineering*,  
13 543 vol. 373, p. 113476, Jan. 2021.
- 14  
15  
16  
17 544 [35] Z.-T. Chang, M. A. Bradford, and R. Ian Gilbert, “Limit analysis of local  
18 545 failure in shallow spherical concrete caps subjected to uniform radial  
19 546 pressure”, *Thin-Walled Structures*, vol. 48, pp. 373–378, June 2010.
- 20  
21  
22  
23  
24 547 [36] Z.-T. Chang, M. A. Bradford, and R. I. Gilbert, “Short-term behaviour  
25 548 of shallow thin-walled concrete dome under uniform external pressure”,  
26 549 *Thin-Walled Structures*, vol. 49, pp. 112–120, Jan. 2011.
- 27  
28  
29  
30  
31 550 [37] A. Zingoni, “Liquid-containment shells of revolution: A review of recent  
32 551 studies on strength, stability and dynamics”, *Thin-Walled Structures*,  
33 552 vol. 87, pp. 102–114, Feb. 2015.
- 34  
35  
36  
37 553 [38] C. Maraveas, G. A. Balokas, and K. D. Tsavdaridis, “Numerical evalua-  
38 554 tion on shell buckling of empty thin-walled steel tanks under wind load  
39 555 according to current American and European design codes”, *Thin-Walled*  
40 556 *Structures*, vol. 95, pp. 152–160, Oct. 2015.
- 41  
42  
43  
44  
45 557 [39] A. Niloufari, H. Showkati, M. Maali, and S. Mahdi Fatemi, “Experimen-  
46 558 tal investigation on the effect of geometric imperfections on the buckling  
47 559 and post-buckling behavior of steel tanks under hydrostatic pressure”,  
48 560 *Thin-Walled Structures*, vol. 74, pp. 59–69, Jan. 2014.
- 49  
50  
51  
52  
53  
54 561 [40] E. Verwimp, T. Tysmans, M. Mollaert, and S. Berg, “Experimental and

- 1  
2  
3  
4  
5  
6  
7  
8  
9  
10 562 numerical buckling analysis of a thin TRC dome”, *Thin-Walled Structures*, vol. 94, pp. 89–97, Sept. 2015.  
11 563  
12  
13  
14 564 [41] E. Verwimp, T. Tysmans, M. Mollaert, and M. Wozniak, “Prediction  
15 565 of the buckling behaviour of thin cement composite shells: Parameter  
16 566 study”, *Thin-Walled Structures*, vol. 108, pp. 20–29, Nov. 2016.  
17  
18  
19  
20 567 [42] D. Zou, J. Sun, H. Wu, Y. Hao, Z. Wang, and L. Cui, “Experimental  
21 568 and numerical studies on the impact resistance of large-scale liquefied  
22 569 natural gas (LNG) storage outer tank against the accidental missile”,  
23 570 *Thin-Walled Structures*, vol. 158, p. 107189, Jan. 2021.  
24  
25  
26  
27  
28  
29 571 [43] F. L. Jiménez, J. Marthelot, A. Lee, J. W. Hutchinson, and P. M. Reis,  
30 572 “Technical brief: knockdown factor for the buckling of spherical shells  
31 573 containing large-amplitude geometric defects”, *ASME Journal of Applied  
32 574 Mechanics*, vol. 84, no. 3, pp. 034501–1–4, 2017.  
33  
34  
35  
36  
37 575 [44] E. Turco and N. L. Rizzi, “Pantographic structures presenting statisti-  
38 576 cally distributed defects: Numerical investigations of the effects on defor-  
39 577 mation fields”, *Mechanics Research Communications*, vol. 77, pp. 65–69,  
40 578 2016.  
41  
42  
43  
44  
45  
46 579 [45] Y. Solyaev, S. Lurie, E. Barchiesi, and L. Placidi, “On the dependence  
47 580 of standard and gradient elastic material constants on a field of defects”,  
48 581 *Mathematics and Mechanics of Solids*, vol. 25, no. 1, pp. 35–45, 2020.  
49  
50  
51  
52 582 [46] L. Placidi, E. Barchiesi, and A. Misra, “A strain gradient variational  
53 583 approach to damage: a comparison with damage gradient models and  
54  
55  
56  
57  
58  
59  
60  
61  
62  
63  
64  
65

- 1  
2  
3  
4  
5  
6  
7  
8  
9  
10 584 numerical results”, *Mathematics and Mechanics of Complex Systems*,  
11 585 vol. 6, no. 2, pp. 77–100, 2018.
- 12  
13  
14 586 [47] L. Placidi and E. Barchiesi, “Energy approach to brittle fracture  
15 587 in strain-gradient modelling”, *Proceedings of the Royal Society A:*  
16 588 *Mathematical, Physical and Engineering Sciences*, vol. 474, no. 2210,  
17 589 p. 20170878, 2018.
- 20  
21  
22 590 [48] U. Mühlich, “Deformation and failure onset of random elastic beam net-  
23 591 works generated from the same type of random graph”, in *Developments*  
24 592 *and Novel Approaches in Biomechanics and Metamaterials* (B. E. Abali  
25 593 and I. Giorgio, eds.), pp. 393–408, Cham: Springer, 2020.
- 28  
29  
30  
31 594 [49] I. Bucur-Horváth and R. V. Săplăcan, “Force lines embodied in the build-  
32 595 ing: Palazzetto dello sport”, *Journal of the International Association for*  
33 596 *Shell and Spatial Structures*, vol. 54, no. 2-3, pp. 179–187, 2013.
- 36  
37  
38 597 [50] P. di Re, E. Lofrano, J. Ciambella, and F. Romeo, “Structural anal-  
39 598 ysis and health monitoring of twentieth-century cultural heritage: the  
40 599 Flaminio Stadium in Rome”, *Smart Structures and Systems*, vol. 27,  
41 600 no. 2, pp. 285–303, 2021.
- 44  
45  
46 601 [51] V. G. Rekach, *Static theory of thin-walled space structures*. Moscow:  
47 602 Mir, 1978.
- 49  
50  
51 603 [52] W. Flügge, *Stresses in shells*. Berlin: Springer, 1960.
- 52  
53  
54 604 [53] S. P. Timoshenko and S. Woinowsky-Krieger, *Theory of plates and shells*.  
55 605 New York: McGraw-Hill, 2nd ed., 1959.

- 1  
2  
3  
4  
5  
6  
7  
8  
9  
606 [54] D. P. Billington, *Thin shell concrete structures*. New York: McGraw-  
10 Hill, 1965.  
11  
12  
13  
608 [55] V. Gioncu, *Thin reinforced concrete shells: special analysis problems*.  
14  
15  
16  
609 Bucarest: Wiley, 1979.  
17  
18  
610 [56] A. M. Haas, *Thin concrete shells*, vol. 1. New York: Wiley, 1962.  
19  
20  
611 [57] A. M. Haas, *Thin concrete shells*, vol. 2. New York: Wiley, 1967.  
21  
22  
23  
612 [58] V. A. Eremeyev and F. dell’Isola, “On weak solutions of the boundary  
24 value problem within linear dilatational strain gradient elasticity for  
25 polyhedral Lipschitz domains”, *Mathematics and Mechanics of Solids*,  
26  
27  
613 p. 108128652110255, 2021.  
28  
29  
30  
31  
32  
616 [59] J.-J. Alibert, P. Seppecher, and F. dell’Isola, “Truss modular beams  
33 with deformation energy depending on higher displacement gradients”,  
34  
35  
617  
36  
618 *Mathematics and Mechanics of Solids*, vol. 8, no. 1, pp. 51–73, 2003.  
37  
38  
39  
619 [60] F. dell’Isola, P. Seppecher, and A. della Corte, “The postulations *à la*  
40 *D’Alembert* and *à la Cauchy* for higher gradient continuum theories  
41  
42  
620 are equivalent: a review of existing results”, *Proceedings of the Royal*  
43  
44  
621  
45  
622 *Society A: Mathematical, Physical and Engineering Sciences*, vol. 471,  
46  
47  
623 p. 20150415, Nov. 2015.  
48  
49  
624 [61] P. Seppecher, J.-J. Alibert, and F. dell’Isola, “Linear elastic trusses lead-  
50  
51  
625 ing to continua with exotic mechanical interactions”, *Journal of Physics:*  
52  
53  
626 *Conference Series*, vol. 319, p. 012018, 2011.  
54  
55  
56  
57  
58  
59  
60  
61  
62  
63  
64  
65

- 1  
2  
3  
4  
5  
6  
7  
8  
9  
627 [62] V. A. Eremeyev, A. Cazzani, and F. dell’Isola, “On nonlinear dilatational  
10 strain gradient elasticity”, *Continuum Mechanics and Thermodynamics*,  
11 vol. 33, pp. 1429–1463, 2021.  
12  
13  
14  
15  
16 [63] F.-F. Wang, H.-H. Dai, and I. Giorgio, “A numerical comparison of the  
17 uniformly valid asymptotic plate equations with a 3D model: Clamped  
18 rectangular incompressible elastic plates”, *Mathematics and Mechanics  
19 of Solids*, p. 108128652110255, 2021.  
20  
21  
22  
23  
24 [64] L. Greco and M. Cuomo, “B-Spline interpolation of Kirchhoff-Love  
25 space rods”, *Computer Methods in Applied Mechanics and Engineering*,  
26 vol. 256, pp. 251–269, 2013.  
27  
28  
29  
30  
31 [65] M. Cuomo, L. Contrafatto, and L. Greco, “A variational model based  
32 on isogeometric interpolation for the analysis of cracked bodies”, *Inter-  
33 national Journal of Engineering Science*, vol. 80, pp. 173–188, 2014.  
34  
35  
36  
37 [66] L. Greco, M. Cuomo, and L. Contrafatto, “A reconstructed local B for-  
38 mulation for isogeometric Kirchhoff–Love shells”, *Computer Methods in  
39 Applied Mechanics and Engineering*, vol. 332, pp. 462–487, 2018.  
40  
41  
42  
43  
44 [67] M. E. Yildizdag, M. Demirtas, and A. Ergin, “Multipatch discontinu-  
45 ous Galerkin isogeometric analysis of composite laminates”, *Continuum  
46 Mechanics and Thermodynamics*, vol. 32, no. 3, pp. 607–620, 2020.  
47  
48  
49  
50  
51 [68] C. Olivieri, M. Angelillo, A. Gesualdo, A. Iannuzzo, and A. Fortunato,  
52 “Parametric design of purely compressed shells”, *Mechanics of Materials*,  
53 vol. 155, p. 103782, Apr. 2021.  
54  
55  
56  
57  
58  
59  
60  
61  
62  
63  
64  
65